RSC Advances

ROYAL SOCIETY OF CHEMISTRY

www.rsc.org/advances

Cite this: DOI: 10.1039/c0xx00000x

www.rsc.org/xxxxxx

ARTICLE TYPE

Cellulose Generated-Microporous Carbon Nanosheets with Nitrogen Doping

Wenzhong Shen,*[a] Tuoping Hu,[a,b] Weibin Fan*[a]

Received (in XXX, XXX) Xth XXXXXXXXX 200X, Accepted Xth XXXXXXXXX 200X

DOI: 10.1039/b000000x

Nanosheet porous carbon with surface area of 1854 m^2/g and pore volume of 0.82 cm^3/g is synthesized using cellulose and KOH/urea, the sheet structure is formed during drying and it was kept after carbonization. The nitrogen-containing groups are incroporated into carbon matrix through urea decomposition and mainly existed as pyridine-like, pyrrole-like and graphite-like nitrogen species. Unique compositional and structural features endow the nitrogen-doped porous carbon nanosheets with superior CO_2 adsorption performance of 5.8 mmol/g.

Introduction

Porous carbon materials are receiving increasing attention because of their potential applications in highly efficient adsorbents,[1] catalysts,[2] and energy materials.[3] They are currently fabricated by carbonization of various carbon precursors or carbon matrix combining with activation or templating technology.[4] The activation using chemicals is to promote the pore developing, while templating is to form pore and control the pore shape.

In addition to the commonly concerned porous feature and surface area, the morphology of porous carbons has also attracted great interest in recent years. Several special morphology endowed porous carbon excellent properties. For example, carbon nanotubes confined metal particles with unique properties in chemical reactions;[5] carbon nanotube with extremely high tensile strength was controlled wall thick by CVD connected with catalyst;[6] Cubic ordered mesostructured carbide-derived carbons offered excellent hydrocarbon storage capacitance and good performance as electrode material for supercapacitors;[7] shell-core structure porous carbon displaying power density of 11.7 KW/kg was obtained using spherical silica as template [8] or controlling phase transferring;[9] nanosheet graphene having excellent reversible capacity of 1040 mAh/g at 100 mA/g was synthesized by controlled low-concentration monomicelle close-packing assembly approach.[10]

Hetroatoms like N and B introduced into porous carbon matrix greatly enhanced electronic chemistry performance due to pseudocapacitive effect,[11] increased adsorption properties for polar molecules because of its basic surface groups,[12] promoted dispersion of catalyst particle and enhanced the interaction of support and catalyst particle,[13] etc.

Recently, some novel synthesis routes to control the morphology of porous carbons were reported, tunable morphologies from micro- to mesoporous with apparent specific surface areas up to 2000 m^2/g was reported by templating salt.[14] Layered porous carbon composed of nano-graphenes was synthesized by using aminoclay as a template.[15] Ultralight carbon nanofiber aerogel with a density of 4-6 mg/cm^3 was derived from bacterial cellulose.[16] Carbon microtube material was synthesized using ZnO as template by CVD process,[17] carbon-based microporous nanoplates containing numerous heteroatoms were fabricated from regenerated silk fibroin,[18] nanosheets of g-C3N4 was obtained through thermal oxidation etching its parent bulk material.[19]

Nanosheet materials, such as, MnO_2, TiO_2, graphene, have been recognized as a novel class of nanostructured materials due to their unique structural feature of ultimate two-dimensional anisotropy with extremely small thickness in nanometer and even subnanometer scale.[20] This characteristic often leads to new physicochemical properties due to the quantum confinement effect.

Hierarchical porous carbon from cotton was prepared in presence of NaOH and urea mixtures [21], and it displayed better properties as catalyst support and electrochemical performances. However, the process needs freeze-dried, and higher ratio of NaOH to cotton, the pore size distribution ranged from micropore to macropore, and the resultant porous carbon was irregular particle.

Herein, we report a facile route to produce high special surface area, large pore volume of nanosheet nitrogen-containing porous carbon from cellulose. When used for CO_2 adsorption, the adsorption capacity is reached up to 5.8 mmol/g at room temperature due to its unique compositional and structural features; it is much higher than reported porous carbon in literatures.

Experimental Section

Synthesis of porous carbon nanosheets

Cellulose was selected as the raw materials for preparing nanosheet porous carbon. In a typical synthesis, after mixing cellulose with mixture solution of KOH and urea (H2O:KOH:Urea:Cellulose=80:8:12:12 wt%), the mixture precursor was dried at 80 ^{o}C, then, it was carbonized in a tube furnace at 600 ^{o}C or 800 ^{o}C for 1 h under nitrogen flow. The obtained sample was subsequently washed in distilled water to remove any metal residue. The samples were noted as C-KU-600 and C-KU-800 according to the carbonization temperature. The pristine cellulose and cellulose impregnated with KOH were also carbonized at 800 ^{o}C and noted as C-O-800 and C-K-800.

Structural Characterization

Nitrogen adsorption/desorption isotherms were measured at -196 oC on a Micromeritics ASAP 2020 adsorption apparatus. Before the measurements, all the samples were degassed at 180 °C for more than 6 h under high vacuum conditions. The surface area was calculated by the Brunauer-Emmett-Teller (BET) method from the adsorption branch in the relative pressure range (P/P0) of 0.01 to 0.2. The pore size distribution (PSD) was calculated by a non-local density functional theory (NLDFT) method using nitrogen adsorption data and assuming a slit pore model. The total pore volumes (Vtotal) were estimated in terms of the adsorption amount at P/P_0 of 0.99. The SEM images were obtained on a S-4800 Field Emission-Scanning Electron Microscope (Hitachi, Japan) operated at 1 KV. Transmission electron microscopy (TEM) was carried out with a JEM-2000 FX instrument operating at a 200 KV accelerating voltage. Fourier transform infrared (FT-IR) spectra of the samples were measured on a Nicolet FT-IR 380 spectrometer using the conventional KBr pellet method. Thermal gravimetric analysis (TGA) was performed under argon at 30-800 ^{o}C with a heating rate of 10 oC/min by A thermogravimetric analyzer (Rigaku, TG-DTA 8120, Japan), and the exhaust gases were detected by subsequent mass spectroscopy (Omni Star). The X-ray photoelectron spectroscopy (XPS) was measured with an ESCALAB 250 (Thermo Electron). The X-ray excitation was provided by a monochromatic Al Kα (1486.6 eV) source. Survey scans were obtained using a pass energy of 100 eV while high resolution scans of specific elements were obtained using a 20 eV pass energy. The detection of the emitted photoelectrons was performed perpendicular to the surface sample. Data quantification was performed on the advantage program.

CO_2-Capture Measurements

The CO_2-adsorption isotherms of the porous carbons were measured using a Micromeritics ASAP 2020 static volumetric analyzer at 25 ^{o}C. Prior to each adsorption experiment, the sample was degassed for 2 h at 150 ^{o}C ensuring that the residual pressure fell below 5×10^{-3} mbar and then cooled down to 25 ^{o}C, followed by the introduction of CO_2 into the system. The CO_2-adsorption capacity in terms of adsorbed volume under standard temperature and pressure (STP) was then recorded.

Results and Discussion

KOH activation has been widely used on grapheme,[22] carbon nanotubes,[23] carbide-derived carbon, and mesoporous carbon [24] to increase the surface area and improve the electrochemical performance. When the activation temperature is higher than 400 °C, The chemical reactions are involved into the process: 6 KOH + 2 C → 2 K + 3 H_2 + 2 K_2CO_3, and subsequent decomposition of K_2CO_3 and/or reactions of $K/K_2CO_3/CO_2$ with the carbon.[25] Given the loss of carbon, a large amount of nanoscale pores are generated in the final products. Scheme 1 outlines the strategy used to synthesize the nanosheet microporous carbon from cellulose. Firstly, cellulose was dispersed into the solution of KOH and urea, the water was evaporated at 80 ^{o}C, the aggregated KOH and urea could further crystallize to form layer structure, and the cellulose coated on the layer surface. Then, the composites were subsequently chemically activated with KOH at 600 ^{o}C or 800 ^{o}C for 1 h under a nitrogen atmosphere, during heating and activation process, the cellulose was performed polymerization and pyrolysis reactions, the urea was decomposed and reacted with carbon and KOH, meanwhile the KOH was reacted with carbon, resulting in porous nitrogen-doped carbon nanosheets with large surface areas. By this pyrolysis, condensation, polymerization, carbonization and activation process, the nitrogen atoms from urea are expected to replace the carbon atoms in the carbon matrix sheets. As illustrated in **Scheme 1**, in this manner, we hope to make use of the better hydrophily of heteroatom-doped carbon materials as well as the open, shortened paths offered by nanosheet microporous carbon materials.

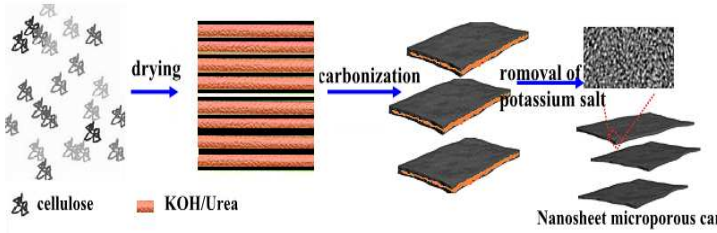

Scheme 1. Description of product and nanosheet formation using the KOH/urea templating approach.

The TGA curves and pyrolysized gases of urea, pristine cellulose, cellulose with urea, cellulose with KOH, and cellulose with KOH/urea showed weight loss in different stages in **Figure 1**. The pyrolysized gases of CO, CO_2, NH_3 and HCN were produced at different temperatures were listed in **Table 1** and the relative intensities vs. temperature were shown in **Figure 1S**. For pristine cellulose, the first stage of weight loss is about 10% in between 50 ^{o}C and 200^{o}C. This may be due to the loss of adsorbed and bound water. The second stage ranged from 200 ^{o}C to 350 ^{o}C with the fastest decomposition rate, 50% weight loss happens due to degradation of cellulose at 350 ^{o}C. A slower weight loss appears from 350 ^{o}C to 700 ^{o}C due to the pyrolysis and decomposition of cellulose to form condensation cross-linking ring structure. For the cellulose with urea, the degradation behavior is different from cellulose. Here, the first stage of weight loss is due to the removal of water content lower at 150 ^{o}C. The onset degradation temperature starts earlier at 150 ^{o}C due to urea decomposing and a fastest weight loss rate occurs from 230 ^{o}C to 320 ^{o}C because of cotton pyrolysis with urea decomposition. When cellulose impregnated with KOH, the weight was gradually decreased from 200 ^{o}C to 500 ^{o}C. The weight loss behavior of cotton impregnated with KOH and urea

showed two fast weight loss rates before 300 °C, the presence of KOH, which promote the decomposition of urea. The carbon yields based on cellulose of pristine cellulose, cellulose with urea, cellulose with KOH, and cellulose with KOH/urea were 13%, 17%, 23% and 25%, respectively. When cellulose impregnated with urea or KOH/urea, the HCN was recorded at higher temperature than that from urea, which indicated that the product of urea might connected with cellulose and was further decomposed to HCN at higher temperature. Based on the exhausted gases forming process, the nitrogen element might be incorporated into carbon matrix via nitrogen radius from urea decomposition during heat treatment.

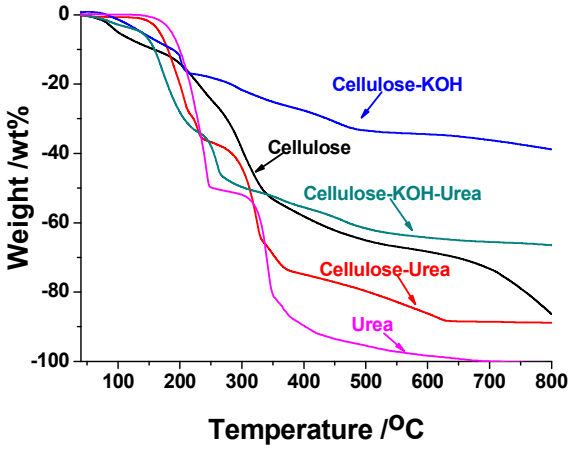

Figure 1. Thermogravimetric analysis of pristine cellulose, cellulose impregnated with urea, KOH, KOH and urea under a nitrogen flow, showing the different stages of decomposition, pyrolysis and activation reaction. Heating rate: 10 °C/min.

The morphologies of the products at different stages were characterized by scanning electron microscopy (SEM) and transmission electron microscopy (TEM) and were shown in **Figure 2** and **Figure 3**. The resulted nanosheet porous carbons obviously maintained their sheet structure, and the thick is about 10 nm (**Figure 2** (e) and (f)). The morphologies of activation products were dependent on the temperature, it is regular piling up after 600 oC activation; but it is irregular assembling after 800 oC activation. When the potassium salt was removed, nanosheet porous carbon with 10-20 nm could be obtained. Compared with cellulose impregnated with KOH or urea, the resulted porous carbons displayed aggregative and irregular particles (see **Figure S2** and **S3**). This result suggests that, as expected, most of the cellulose are concentrated on the surface of KOH and urea during drying process, thus the morphology of residual carbon are kept after activation. The HRTEM image in **Figure 3** (b) and (d) indicate that nanosheet porous carbon of C-KU-600 and C-KU-800 mainly contained micropore less than 2 nm, classical structure of biomass carbon. **Figure 4S** displayed different magnification of C-KU-600 and C-KU-800. Meanwhile, the nanosheet was twisted of C-KU-800; this was possible of serious reaction between KOH and carbon at high temperature.

The specific surface areas and pore size distributions of samples were measured by N_2 adsorption-desorption isotherms (**Figure 4** (a)). The pore structure parameters of samples were listed in **Table 2**. The nanosheet carbons exhibited type I isotherms, and a high Brunauer-Emmett-Teller surface area of 1854 m^2/g for C-KU-800 and 1138 m^2/g for C-KU-600. The pore size distribution curves derived from the adsorption branch of isotherms using nonlocal density functional theory (NLDFT) method are presented in **Figure 4** (b). The C-KU-800 with a high pore volume of 0.82 cm^3/g mainly possesses micropores (peak at 0.74, 1.10 and 1.74 nm); and showed stronger pore size distributions intensities in 0.9-1.1nm and 1.7-3 nm than that of C-KU-600, this is again corroborated the HRTEM results. Compared with C-K-800 (surface area of 1436 m^2/g and pore volume of 0.697 cm^3/g), the higher surface area and pore volume of C-KU-800 may be resulted from the dispersion of cellulose with KOH/urea, and the resultant porous carbon morphology. Although porous carbon from pristine cellulose displayed type I isotherm, it showed lower surface area (460 m^2/g) and less pore volume (0.22 cm^3/g), this indicated that the cellulose impregnated with KOH and urea, could evolve nanosheet structure and promote the pore structure developing.

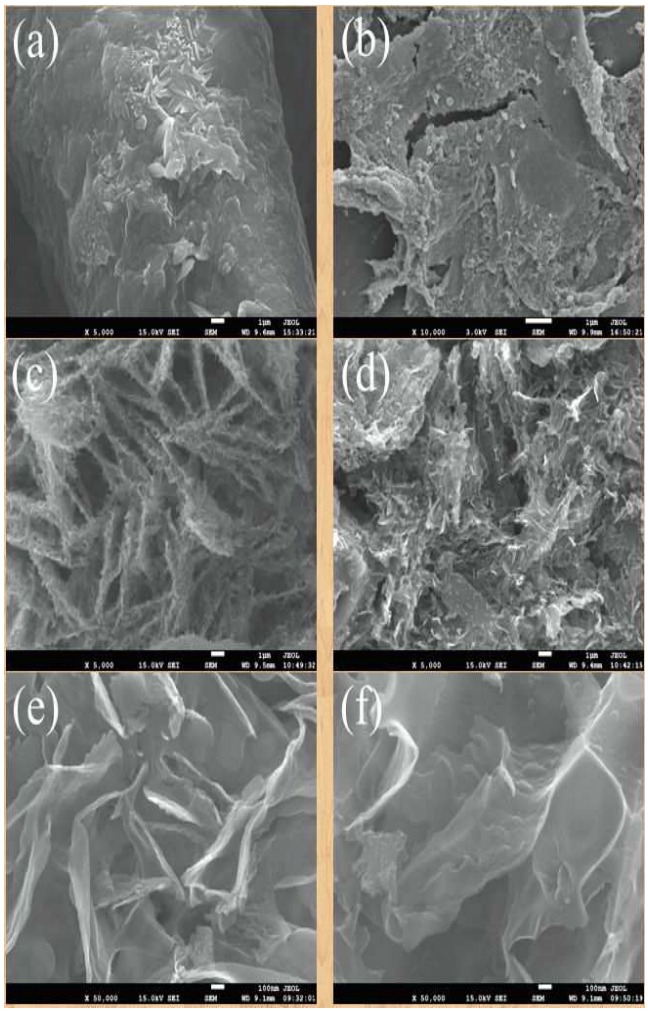

Figure 2. SEM images of cellulose impregnated KOH/urea at different stages. (a) and (b) cellulose KOH/urea composites; (c) activated at 600 °C without leaching; (d) activated at 800 °C without leaching; (e) nanosheet porous carbon activated at 600 °C after leaching and (f) nanosheet porous carbon activated at 800 °C after leaching.

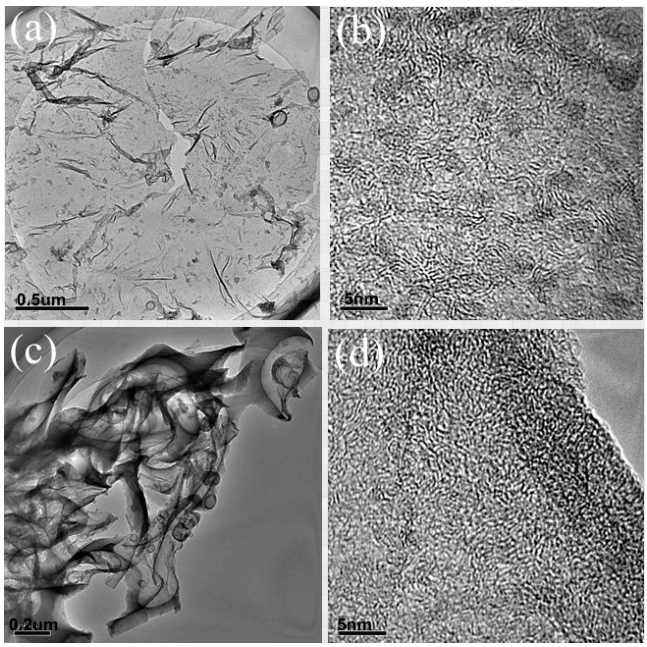

Figure 3. HRTEM images of nanosheet porous carbons at different resolutions. (a) and (b) C-KU-600; (C) and (D) C-KU-800.

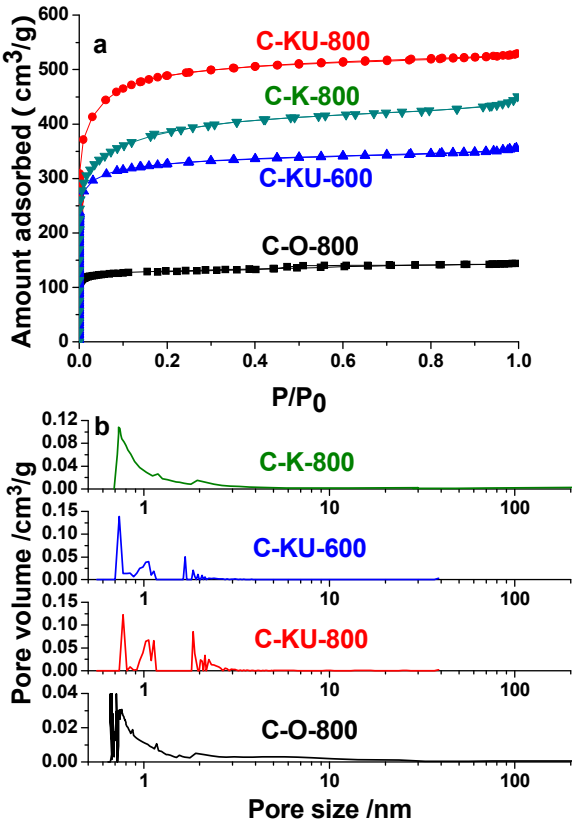

Figure 4. a) N_2 sorption isotherms and b) NLDFT pore size distributions of samples (C-O-800, C-K-800, C-KU-600 and C-KU-800).

The Fourier transformed infrared (FT-IR) spectra of pristine cellulose, C-O-800, C-KU-600 and C-KU-800 were shown in **Figure S5**, in which the main absorption peaks of functional groups, such as C=O, C-O, C-H, and -O-H, gradually became weak and finally disappeared with carbonization temperature, thereby indicating the carbonization temperature increase promotes the surface hydrophobic.

To confirm the chemical composition, X-ray photoelectron spectroscopy (XPS) and elemental analysis were conducted. As shown in **Figure 5** and **Figure S6**, three typical peaks corresponding to the binding energies of C 1s, N 1s, and O 1s are observed in the wide XPS survey scan for C-KU-600 and C-KU-800. In contrast to C-KU-600, the N1s peak is weak in C-KU-800. Three types of nitrogen configurations and related contents: pyridine-like (N-6), pyrrole-like (N-5), and graphite-like (N-Q) were illustrated in C-KU-600 and C-KU-800 (**Figure 6** and **Table S1**). The three nitrogen configurations related peaks area ratio for C-KU-600 and C-KU-800 were 1.69:1.82:1 and 2.27:2.60:1, respectively. Quantitative analysis elucidates the corresponding atom contents (Table 2) were consistent with that derived from elemental analysis. Moreover, the contents of pyridine-like (N-6) and pyrrole-like (N-5) increased, but the graphite-like (N-Q) decreased with activation temperature. This discrepancy is in accordance with the previous observation that the nitrogen functional groups are decreased with activation temperature.[26]

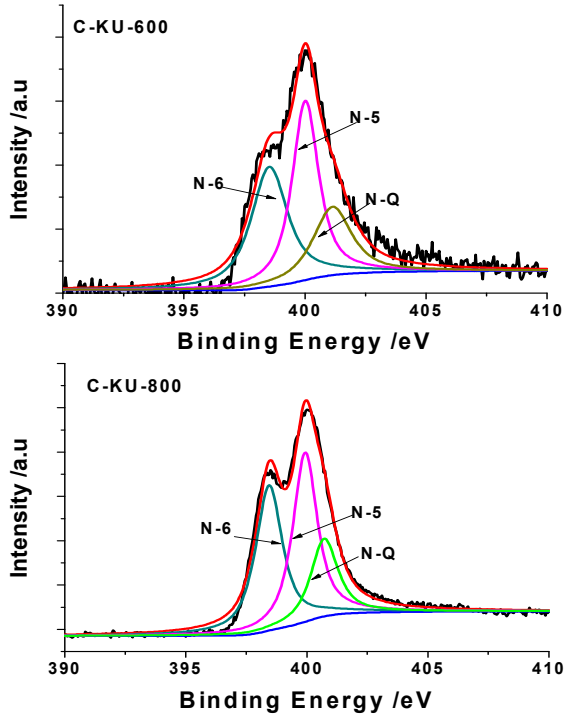

Figure 5. High-resolution N1s XPS spectra of C-KU-600 and C-KU-800.

The C 1s XPS spectra obtained for C-KU-600 and C-KU-800, showed rather complex deconvoluted patterns (**Figure S6**). Both C-KU-600 and C-KU-800 exhibited a broad peak at 284.6 eV and this peak could be deconvoluted into several distinct peaks at 284.6, 285.7 and 288.2 eV for C-KU-600 and 284.3, 284.6, 285.6, 286.6, and 288.3 eV for C-KU-800, this revealed the presence of signals from C=C (284.6 eV), C–O or C–N (285.7 eV), C=O or C=N (288.2 eV). In addition, the O 1s peaks of C-KU-600 and C-KU-800 (**Figure S6**), which can be

ascribed to adsorbed oxygen (531.2 eV), =C=O/–C–O–C–(532.2 eV), –O–C=O (533.2 eV), respectively.[27]

The above characterizations proved the existence of oxygen and nitrogen-containing groups in the nanosheet microporous carbons prepared from cellulose. Its adsorption isotherms of CO_2 were drawn in **Figure 6** (a), the CO_2 uptakes by C-K-800, C-KU-600 and C-KU-800 were 4.1 mmol/g, 5.0 mmol/g and 5.8 mmol/g, respectively. Compared with the reported cellulose-based high surface area porous carbon (S_{BET}=2250m^2/g, V_{total}=1.01cm^3/g) [28], the nanosheet porous carbon had less surface area and pore volume, but its CO_2 adsorption capacity was same to that of high surface area porous carbon (5.8mmol/g), this indicated that the nitrogen doping nanosheet porous carbon was potential materials for CO_2 capture due to its unique compositional and structural features. Moreover, the adsorption capacity of CO_2 was 2.0 mmol/g at 0.15 bar, it is interesting for flue gas CO_2 capture. **Figure 6** (b) shows the CO_2-TPD profiles of C-KU-600 C-KU-800, there are three desorption peaks appearing before 150 °C, 150-230 °C and 230-300 °C, which represent the physical adsorbed CO_2, poor and strong chemical adsorbed CO_2. The TPD-CO_2 of C-K-800 illustrated that there was mainly physical adsorption due to no nitrogen-containing groups on its surface. This suggested that large surface area, pore volume and surface rich of basic sites are necessary for achieving high CO_2 adsorption capacity.

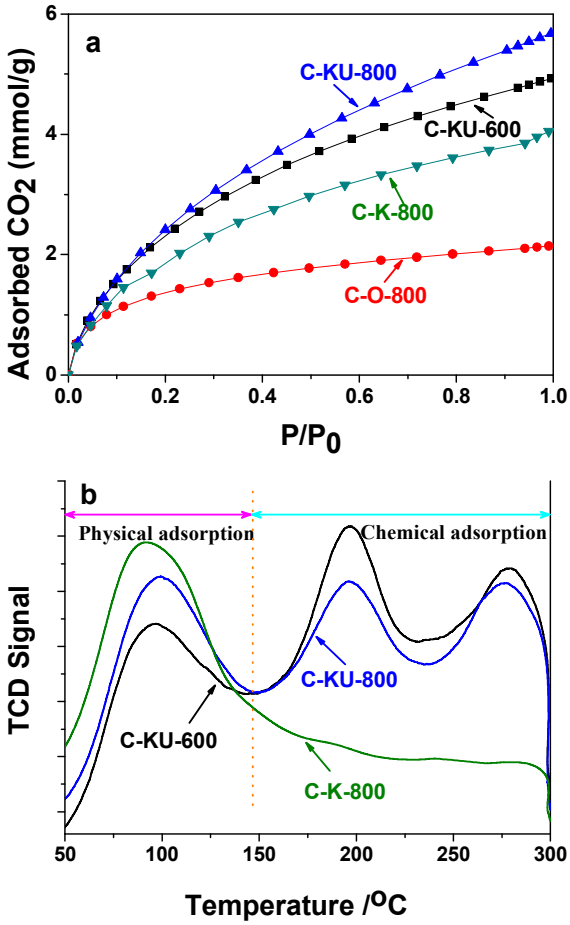

Figure 6. (a) CO_2 adsorption isotherms of C-O-800, C-K-800, C-KU-600 and C-KU-800; (b) CO_2-TPD curves of C-K-800, C-KU-600 and C-KU-800.

Physical adsorption for CO_2 was mianly taken place at micropore range of porous carbon,[29] C-KU-800 showed higher surface area and pore volume than that of C-KU-600, but the difference of their microporous volume is less (0.53 cm^3/g vs. 0.45 cm^3/g). The nitrogen content of C-KU-600 is 2.6 times of C-KU-800 (3.57 wt% vs. 1.37 wt%), and it has more N-Q species, so, a higher CO_2 desorption peak of C-KU-600 appears between 250 °C and 300 °C. In addition, the nitrogen groups in external surface and large pore wall of C-KU-600 and C-KU-800 may adsorb CO_2. Compared with C-KU-800 and C-K-800, C-KU-600 with less surface area and mircroporous volume, but it still displayed better adsorption property for CO_2 due to its more nitrogen groups. Summarized above factors, CO_2 adsorption was determined by the micropous structure and surface nitrogen groups.

In order to compare the effect of NaOH and KOH on the pore structure and morphology of cellulose-based porous carbon, the cellulose was impregnated with NaOH and urea (same molar ratio as KOH), and was activated at 800 °C. The nitrogen adsorption isotherm, CO_2 adsorption isotherm and morphology of resultant porous carbon (C-NaU-800) were showed in **Figure S7-S9**. The special surface area and pore volume of porous carbon from cellulose impregnated with NaOH/urea are less than that of C-KU-800; its pore size distribution is wider than that of C-KU-800. In general, KOH produces porous carbons with narrower micropore distributions than those prepared by NaOH [30]. The C-NaU-800 is irregular particles; this may be determined by the chemical property of NaOH. The CO_2 adsorption capacity on C-NaU-800 reached to 4.5 mmol/g, but the adsorption isotherm was gentler than that of C-KU-800 and C-KU-600, this suggested that the pore structure and morphology determined the CO_2 adsorption behavior on porous carbons. The nanosheet structure minimizes CO_2 diffusion limitations and allows rapid adsorption.

Table 1 Exhausting temperature ranges and relative percent contents of CO, CO_2, HN_3, HCN from urea, pristine cellulose, cellulose impregnated with urea, KOH, KOH and urea during heating in Ar flow

Samples	Temperature (°C)				Exhausted gases relative content (%)			
	CO	CO_2	NH_3	HCN	CO	CO_2	NH_3	HCN
Urea	150-300	170-240; 280-350; 360-650	150-300	300-370	16.03	53.44	29.75	0.78
Cellulose	250-350	250-350	-	-	48.95	49.94	-	-
Cellulose-Urea	150-370	150-225; 250-400	150-250; 350-500	300-550; 550-800	30.82	36.69	28.99	3.49
Cellulose-KOH	200-350; 350-450; 600-800	170-270; 410-470; 550-800	-	-	61.93	37.46	-	-
Cellulose-KOH-Urea	170-280; 370-450; 600-800	150-250; 250-400; 500-750	170-250; 250-400	250-570; 650-800	40.54	36.14	22.09	0.93

Table 2 Chemical composition and structure parameters of samples

Samples	Elemental composition (wt%)[a*]				Structure parameter			
	C	H	N	O	S_{BET} m^2/g [b*]	S_{Micro} m^2/g [c*]	V_{total} cm^3/g [d*]	V_{Micro} cm^3/g
C-800	92.73	0.552	-	6.72	460	419	0.22	0.18
C-K-800	91.94	0.45	-	7.61	1436	1238	0.697	0.446
C-KU-600	83.18	0.82	3.57	12.43	1138	894	0.55	0.45
C-KU-800	88.75	0.80	1.37	9.08	1854	1351	0.82	0.53

a) Data from elemental analysis, b) Specific surface area from multiple BET method; c) Micropore surface area from t-plot method; d) Total pore volume at P/P_0=0.99).

Conclusions

Nitrogen-doped porous carbon sheets are successfully fabricated via chemical activation of cellulose impregnated with KOH and urea. Unique compositional and structural features endow the nitrogen-doped porous carbon nanosheets with superior CO_2 adsorption performance of 5.8 mmol/g.

Notes and references

a State Key Laboratory of Coal Conversion, Institute of Coal Chemistry, Chinese Academy of Sciences, Taiyuan , Shanxi , 030001, PR China,Fax: +86-351-4041153, E-mail: shenwzh2000@yahoo.com.

[b] Northern University of China, Taiyuan, Shanxi 030051, P.R. China

† Electronic Supplementary Information (ESI) available: [Exhaust gases compositions, FT-IR spectra, SEM images of the cellulose with urea or KOH, TEM images of nanosheet porous carbons, C1s and O1s XPS spectra, and different nitrogen group contents]. See DOI: 10.1039/b000000x/

1. a) S. H. Joo, S. J. Choi, I. Oh, J. Kwak, Z. Liu, O. Terasaki, R. Ryoo, *Nature* **2001**, *412*, 169; b) C. D. Liang, Z. J. Li, S. Dai, *Angew. Chem., Int. Ed.* **2008**, *47*, 3696; c) Y. Wan, Y. F. Shi, D. Y. Zhao, *Chem. Mater.* **2008**, *20*, 932.
2. a) X. Wang, J. C.Yu, Y. Hou, X. Fu, *Adv. Mater.* **2005**, *17*, 99; b) S. E. Skrabalak, K. S. Suslick, *J. Am. Chem. Soc.* **2005**, *127*, 9990.
3. J. P. Paraknowitsch, J. Zhang, D. Su, A. Thomas, M. Antonietti, *Adv. Mater.* **2010**, *22*, 87.
4. K. J. Lee, N. Shiratori, G. H. Lee, J. Miyawaki, I. Mochida, S. H. Yoon, J. Jang, *Carbon* **2010**, *48*, 4248
5. D. H. Deng, L.Yu, X. Q. Chen, G. X. Wang, L. Jin, X. L. Pan, J. Deng, G. Q. Sun, X. H. Bao, *Angew. Chem. Int. Ed.* **2013**, *52*, 371.
6. a) X. H. Zhong, Y. L. Li, J. M. Feng, *Nanoscale* **2012**, *4*, 5614; b) Z. Shi, X. J. Chen, X. W. Wang, Ting Zhang, J. Jin, *Adv. Funct. Mater.* **2011**, *21*, 4358.
7. M. Oschatz, E. Kockrick, M. Rose, L. Borchardt, N. Klein, I. Senkovska, T. Freudenberg, Y. Korenblit, G. Yushin, S. Kaskel, *Carbon* **2010**, *48*, 3987.
8. F. J. Li, M. Morris, Kwong-Yu Chan, *J. Mater. Chem.* **2011**, *21*, 8880.
9. Y. B. Jiang, L. H. Wei, Y. Z. Yu, T. Zhao, *Exp Polym. Lett.* **2007**, *1*, 292.
10. Y. Fang, Y. G. Lv, R. C. Che, H. Y. Wu, X. H. Zhang, D. Gu, G. F. Zheng, Dongyuan Zhao, *J. Am. Chem. Soc.* **2013**, *135*, 1524.
11. a) H.G. Wang, Z. Wu, F. L. Meng, D. L. Ma, X. L. Huang, L. M. Wang, Xin-bo Zhang, *Chemsuschem* **2013**, *6*, 56; b) F. Su, C. K. Poh, J. S. Chen, G. Xu, D. Wang, Q. Li, J. Lin, X. W. Lou, *Energy Environ. Sci.* **2011**, *4*, 717.
12. a) W. Z. Shen, S. C. Zhang; Y. He; J. F. Li, W. B. Fan, *J. Mater. Chem.* **2011**, *21*, 14036; b) R. Ansari, N. K. Fahim, *React. Funct. Polym.* **2007**, *67*, 367
13. a) Y. Wang, J. Yao, H. Li, D. Su, M. Antonietti, *J. Am. Chem. Soc.* **2011**, *133*, 2362; b) K. Chizari, A. Deneuve, O. Ersen, I. Florea,Y. Liu, D. Edouard, I. Janowska, D. Begin, C. Pham-Huu, *Chemsuschem* 2**012**, *5*, 102.
14. N. Fechler, T. P. Fellinger, M. Antonietti, *Adv. Mater.* **2013**, *25*, 75.
15. K. K. R. Datta, D. Jagadeesan, C. Kulkarni, A. Kamath, R. Datta, M. Eswaramoorthy, *Angew. Chem. Int. Ed.* **2011**, *50*, 3929.
16. Z. Y. Wu, C. Li, H. W. Liang, J. F. Chen, S. H. Yu, Angew. *Chem. Int. Ed.* **2013**, *52*, 2925.

17. M. Mecklenburg, A. Schuchardt, Y. K. Mishra, S. Kaps, R. Adelung, A. Lotnyk, L. Kienle, Karl Schulte, *Adv. Mater.* **2012**, *24*, 3486.
18. Y. S. Yun, S. Y. Cho, J. Shim, B. H. Kim, S. J. Chang, S. J. Baek, Y. S. Huh, Y. Tak, Y. W. Park, S. Park, H. J. Jin, *Adv. Mater.* **2013**, *25*, 1993.
19. P. Niu, L. L. Zhang, G. Liu, H. M. Cheng, *Adv. Funct. Mater.* **2012**, *22*, 4763.
20. a) T. Sasaki, M. Watanabe, H. Hashizume, H. Yamada, H. Nakazawa, *J. Am. Chem. Soc.* **1996**, *118*, 8329; b) Y. Omomo, T. Sasaki, L. Z. Wang, M. Watanabe, *J. Am. Chem. Soc.* **2003**, *125*, 3568; c) S. Ithurria, M. D. Tessier, B. Mahler, R. P. S. M. Lobo, B. Dubertret, Al. L. Efros, *Nat. Mater.* **2011**, *10*, 936; d) A. K. Geim, K. S. Novoselov, *Nat. Mater.* **2007**, *6*, 183.
21. a) Y. S. Yun, J.Shim, Y.Tak, H. J. Jin, *RSC Adv.* **2012**, *2*, 4353-4358, b) Y. S. Yun, D. Kim, H. H. Park, Y. Tak, H. J. Jin, *Synth. Met.* **2012**, *162*, 2337-2341, c) Y. S. Yun, H. J. Jin, *Mater. Lett.* **2013**, *108*, 311-315
22. Y. W. Zhu, S. Murali, M. D. Stoller, K. J. Ganesh, W. W. Cai, P. J. Ferreira, A. Pirkle, R. M. Wallace, K. A. Cychosz, M. Thommes, D. Su, E. A. Stach, R. S. Ruoff, *Science* **2011**, *332*, 1537.
23. E. Raymundo-Piñero, P. Azaïs, T. Cacciaguerra, D. Cazorla-Amorós, A. Linares-Solano, F. Béguin, *Carbon* **2005**, *43*, 786.
24. J. Jin, S. Tanaka, Y. Egashira, N. Nishiyama, *Carbon* **2010**, *48*, 1985.
25. M. A. Lillo-Ródenas, D. Cazorla-Amorós, A. Linares-Solano, *Carbon* **2003**, *41*, 267.
26. a) M. Molina-Sabio, F. Rodríguez-Reinoso, *Colloids Surf. A* **2004**, *24*, 15; b) L. Zhao, L. Z. Fan, M. Q. Zhou, H. Guan, S. Qiao, M. Antonietti, M. M. Titirici, *Adv. Mater.* **2010**, *22*, 5202.
27. J. F. Moulder, W. F. Stickle, P. E. Sobel, K. D. Bomben, *Handbook of X-Ray Photoelectron Spectroscopy - A Reference Book of Standard Spectra for Identifi cation and Interpretation of XPS Data*, Perkin-Elmer Corporation, Eden Prairie, MN, USA **1992**.
28. M. Sevilla, A.B. Fuertes, Energy Environ. Sci. **2011**, *4*, 1765.
29. H. R. Wei, S. B. Deng, B. Y. Hu, Z. H.; Chen, B. Wang, J. Huang, G. Yu, *Chemsuschem* **2012**, *5*, 2354.
30. P.J.M. Carrott, M.M.L. Ribeiro Carrott, Suhas, Carbon **2010**, 48, 4162.

Graphical abstract

Nanosheet porous carbon with high surface area and pore volume, Unique compositional and structural features endow the nitrogen-doped porous carbon nanosheets with superior CO_2 adsorption performance.